Received: 7 December 2022 | Revised: 28 March 2023 | Accepted: 29 March 2023

DOI: 10.1111/tra.12886

RESEARCH ARTICLE

Traffic WILEY

Pseudophosphatase STYXL1 depletion enhances glucocerebrosidase trafficking to lysosomes via ER stress

Saloni Patel | Anshul Milap Bhatt | Priyanka Bhansali | Subba Rao Gangi Setty

Department of Microbiology and Cell Biology, Indian Institute of Science, Bangalore, India

Correspondence
Subba Rao Gangi Setty, Department of Microbiology and Cell Biology, Indian Institute of Science, CV Raman Avenue, Bangalore 560012 India.
Email: subba@iisc.ac.in

Funding information
Department of Biotechnology, Ministry of Science and Technology, India, Grant/Award Numbers: BT/PR4982/AGR/36/718/2012, BT/PR32489/BRB/10/1786/2019; Science and Engineering Research Board, Grant/Award Number: CRG/2019/000281; The Wellcome Trust DBT India Alliance, Grant/Award Number: 500122/Z/09/Z; National Bioscience Award, Grant/Award Number: BT/HRD-NBA-NWB/38/2019-20; DBT-JRFs, Grant/Award Number: DBT/2015/IISc/NJ-02 and DBT/2016/IISc/717

Abstract

Pseudophosphatases are catalytically inactive but share sequence and structural similarities with classical phosphatases. STYXL1 is a pseudophosphatase that belongs to the family of dual-specificity phosphatases and is known to regulate stress granule formation, neurite formation and apoptosis in different cell types. However, the role of STYXL1 in regulating cellular trafficking or the lysosome function has not been elucidated. Here, we show that the knockdown of STYXL1 enhances the trafficking of β-glucocerebrosidase (β-GC) and its lysosomal activity in HeLa cells. Importantly, the STYXL1-depleted cells display enhanced distribution of endoplasmic reticulum (ER), late endosome and lysosome compartments. Further, knockdown of STYXL1 causes the nuclear translocation of unfolded protein response (UPR) and lysosomal biogenesis transcription factors. However, the upregulated β-GC activity in the lysosomes is independent of TFEB/TFE3 nuclear localization in STYXL1 knockdown cells. The treatment of STYXL1 knockdown cells with 4-PBA (ER stress attenuator) significantly reduces the β-GC activity equivalent to control cells but not additive with thapsigargin, an ER stress activator. Additionally, STYXL1-depleted cells show the enhanced contact of lysosomes with ER, possibly via increased UPR. The depletion of STYXL1 in human primary fibroblasts derived from Gaucher patients showed moderately enhanced lysosomal enzyme activity. Overall, these studies illustrated the unique role of pseudophosphatase STYXL1 in modulating the lysosome function both in normal and lysosome-storage disorder cell types. Thus, designing small molecules against STYXL1 possibly can restore the lysosome activity by enhancing ER stress in Gaucher disease.

KEYWORDS
ER stress and Gaucher disease, lysosome, pseudophosphatase, STYXL1, TFE3, TFEB, β-glucocerebrosidase

1 | INTRODUCTION

Phosphatases regulate several cell signaling pathways by dephosphorylating specific targets such as lipids, carbohydrates and proteins that participate in these pathways.[1–3] Cell harbors a class of pseudophosphatases, which share sequence and structural similarity with classical phosphatases but lack amino acid residues important for their catalytic activity.[4–6] Pseudophosphatases have been shown to play an indirect role in modulating cell signaling by regulating the activity of other phosphatases. Additionally, these molecules can sequester the substrate or activate/inhibit the action of other phosphatases by acting as their cofactor or even dimerizing with them or

Saloni Patel and Anshul Milap Bhatt contributed equally to this study.

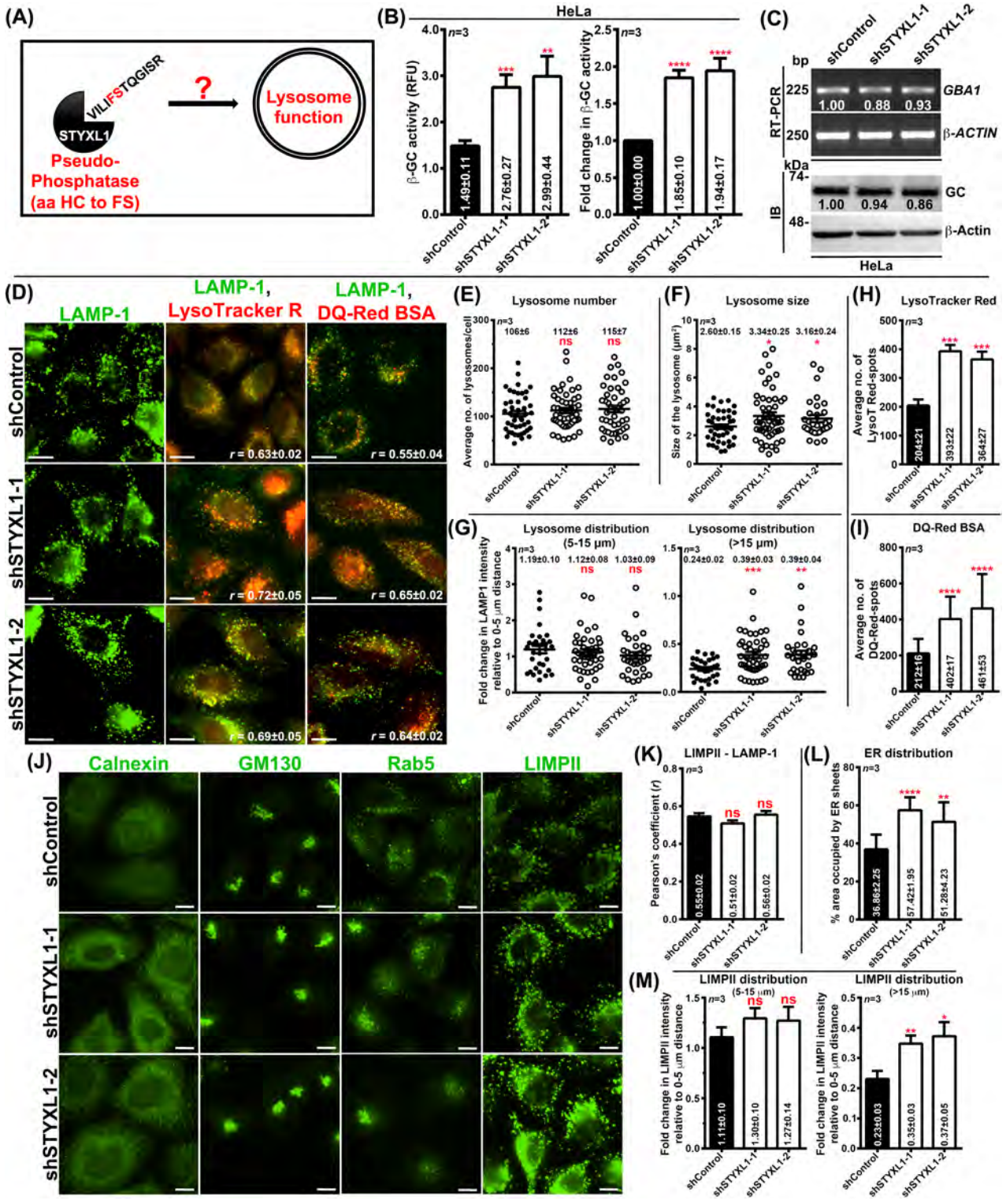

FIGURE 1 Legend on next page.

act as anchors to interact with the components of different signaling pathways.[4–6] Hence these pseudophosphatases possibly play a key role in altering signaling pathways either directly or indirectly.

Based on the sequence similarity, the maximum member of pseudophosphatases belongs to the protein tyrosine phosphatase (PTP) family.[5,7] These phosphatases are further divided into classical pTyr-specific and dual-specificity phosphatases depending on the type of phosphorylation sequence found on their respective substrates.[5,8,9] STYXL1 (serine/threonine/tyrosine-interacting like 1; also known as map kinase phosphatase-like protein, STYX, MK-STYX or DUSP24)

belongs to the later subclass and contains phenylalanine (F) and serine (S) residues in place of histidine (H) and cysteine (C) respectively, found in the active site of classical phosphatases (Figure 1A).[10] Interestingly, reversal of FS to HC residues renders the STYXL1 into catalytically efficient pseudophosphatase.[10] Functionally, STYXL1 has been shown to inhibit stress granule formation by forming a complex with G3BP1.[10] STYXL1 has also been shown to regulate the ERK1/2 signaling required for cell migration and differentiation of PC12 cells and its depletion causes Golgi fragmentation.[11] Furthermore, the STYXL1 knockdown in HeLa cells renders resistance to apoptosis under cellular stress conditions.[12] Subsequent studies have shown an interaction of STYXL1 with PTPM1 phosphatase, which modulates apoptosis[13] and with FBXW7 inhibits its substrate binding.[14] At the cellular level, STYXL1 has been implicated in inducing the formation of neurite-like outgrowth in PC12 cells in a RhoA-dependent manner.[15] Recently, a role for STYXL1 in enhancing the detyrosinization of microtubules through HDAC6 has been reported.[16] However, the role of STYXL1 in regulating the function of subcellular compartments such as lysosomes or ER has not been reported.

Lysosomes are the key homeostatic organelle in all eukaryotic cells and regulate various cellular processes, including degradation. The digestion of cellular materials in lysosomes is mediated through a set of enzymes called acid hydrolases, which are synthesized in ER and transported to lysosomes via Golgi.[17] Any defects in the function of lysosomal enzymes result in the accumulation of substrate that causes lysosomal storage disorders (LSDs).[18] One such enzyme is β-glucocerebrosidase (β-GC, code for *GBA1*, EC 3.2.1.45),[19] which degrades glucosylceramide into glucose and ceramide at acidic pH with the help of its cofactor saposin C.[20] Around 300 different mutations were reported in β-GC, and they are known to cause Gaucher disease[21] with clinical phenotypes splenomegaly or hepatomegaly and sometimes associated with the central neural system.[22] The most common Gaucher disease mutations observed in β-GC are N370S, L444P or G202R, which undergo improper folding and endoplasmic reticulum (ER)-associated degradation.[23–25] Our objective is to delineate the cellular molecules which can directly or indirectly facilitate the folding and trafficking of β-GC to lysosomes and enhance its activity. With this aim, we have performed an RNAi screen against the genome-wide phosphatome to enhance lysosome enzyme activity, which identified STYXL1 as a potential hit.[26] Nevertheless, it is unknown how STYXL1 depletion improves the function of lysosomes. Here, we show for the first time that the knockdown of STYXL1 in HeLa cells enhanced the trafficking of β-GC (wild-type [WT] and Gaucher mutant) from ER to lysosomes and increased its activity. Further, depletion of STYXL1 displayed moderately enhanced ER stress and dispersion of ER and lysosomes with increased contacts between them. In a nutshell, our studies demonstrated a role for pseudophosphatase STYXL1 in altering the lysosome function both in normal and Gaucher patient cells and forming a potential drug target for this genetic disease.

2 | RESULTS

2.1 | STYXL1 knockdown enhances the lysosomal β-glucocerebrosidase activity

The pseudophosphatase STYXL1 shares a common signature motif (VILIFSTQGISR) with dual-specificity phosphatases of the PTP superfamily (Figure 1A).[9] The signature motif of PTP family phosphatases possesses histidine (H) and cysteine (C), which are required for the dephosphorylation activity. Interestingly, STYXL1 contains phenylalanine (F) and serine (S) in place of H and C, respectively, which makes the phosphatase a pseudo enzyme/phosphatase (Figure 1A).[10] Consistently, studies have shown that reversal of FS to HC in STYXL1 (also called MK-STYX) restored the catalytic activity.[10]

Large-scale RNAi screen using pooled shRNAs against the human phosphatome in HeLa cells identified STYXL1 as a hit, whose knockdown displayed enhanced lysosomal β-GC activity.[26] In this study, we questioned the role of STYXL1 pseudophosphatase in modulating the lysosome function (Figure 1A). To analyze the effect of STYXL1 knockdown in regulating the lysosome enzyme activity, we have chosen two shRNAs (referred to here as shSTYXL1-1 and shSTYXL-2) from the available five shRNAs in the phosphatome library (Sigma-Aldrich, SH0411) and non-mammalian shRNA (Sigma-Aldrich, SHC002, referred to here as shControl) as a control in all our

FIGURE 1 Depletion of STYXL1 enhances β-GC activity and alters the distribution of proteolytically active lysosomes, late endosomes and ER network in HeLa cells. (A) Pictorial diagram questioning the role of pseudophosphatase STYXL1 in lysosome function. The diagram displays the active site residues of STYXL1, which contains phenylalanine (F) and serine (S) in the place of histidine (H) and cysteine (C), present in the signature motif (mediates the dephosphorylation) of PTP family phosphatases. (B) Plot representing the β-GC activity in control shRNA (shControl) or two different STYXL1 (shSTYXL1-1 and shSTYXL1-2) shRNAs transfected HeLa cells. β-GC activity in relative fluorescence units (RFUs) and fold change with respect to the control are plotted separately as mean ± s.e.m., $n = 3$. (C) Semi-quantitative RT-PCR and immunoblotting analysis of control and STYXL1-depleted HeLa cells for the expression of *GBA1* transcripts and glucocerebrosidase (GC) protein. β-actin is used as a loading control. The normalized fold change in the transcript/protein levels with respect to control is indicated on the blots. (D, J) IFM analysis of control and STYXL1 knockdown HeLa cells that were stained with indicated antibodies or LysoTracker Red or internalized with DQ-Red BSA. The colocalization efficiency between the markers is indicated as Pearson's coefficient (*r*) value or plotted in (K). Scale bars, 10 μm. (E, F) Quantification of lysosome number (E) and size (F) in the cells. (H, I) Quantification of a number of LysoTracker Red (H) or DQ-Red (I) puncta in the cells. (G, L, M) Quantification of the distribution of lysosomes (LAMP-1), late endosomes (LIMPII) and ER in the cells. In (G) and (M), the fold change in organelles distribution between 5-15 μm or more than 15 μm with respect to 0–5 μm was plotted. The average values in mean ± s.e.m. are indicated in all graphs. ns = not significant, $*p \le 0.05$, $**p \le 0.01$, $***p \le 0.001$ and $****p \le 0.0001$. ER, endoplasmic reticulum; IFM, immunofluorescence microscopy.

experiments. Further, we have used a biochemical assay β-GC activity as a measure of lysosome function in HeLa cells (described in Section 4).[27] The knockdown of STYXL1 (using shSTYXL1-1 and shSTYXL-2 separately) in HeLa cells showed an increased β-GC activity by more than 1.9 folds compared to control cells (Figure 1B). To validate the depletion of STXYL1 in HeLa cells, we have measured the transcript levels of STYXL1 by semi-quantitative PCR and found a reduction of approximately 50% transcripts in the shSTYXL1 cells compared to the shControl cells (Figure S1A). However, the validation of STYXL1 knockdown by immunoblotting was inconclusive because of non-specificity of the anti-STYXL1 antibody (Figure S1A). We hypothesized that the enhanced β-GC activity might be because of the increased β-GC transcripts and/or protein levels in the STYXL1-depleted cells. The transcript and protein levels of β-GC (*GBA1* and GC, respectively) were unaffected significantly in the shSTYXL1 cells compared to the shControl cells (Figure 1C). Thus, these studies suggest that STYXL1 knockdown in HeLa cells modulates the β-GC activity without affecting the transcript or protein levels of β-GC.

2.2 | STYXL1 knockdown disperses the ER, late endosomes and lysosomes and increases the lysosome size, acidity and cargo degradation

To test the effect of STYXL1 knockdown on different organelles, we performed immunofluorescence microscopy (IFM) of STYXL1-depleted HeLa cells with organelle-specific markers. Imaging analysis showed an increased number of peripheral lysosomes (positive for LAMP-1) in STYXL1 knockdown compared to control HeLa cells (Figure 1D). Quantitative analysis showed significantly enhanced lysosome size (∼1.3-fold; sh1: 3.34 ± 0.25 μm^2, sh2: 3.16 ± 0.24 μm^2 and C: 2.60 ± 0.15 μm^2) but not the number in shSTYXL1 compared to shControl cells (Figure 1E,F). As expected, the fold change in lysosomes distribution was significantly increased in the peripheral area above 15 μm distance (∼1.6-fold; sh1: 0.39 ± 0.03, sh2: 0.39 ± 0.04 and C: 0.24 ± 0.02) but not between 5-15 μm distance in comparison to 0–5 μm distance from the center of the cell (Figure 1G). Studies have shown that peripheral lysosomes are less acidic than perinuclear localized lysosomes.[28,29] Therefore, we tested the acidity and cargo processivity of lysosomes in STXYL1 knockdown cells. IFM analysis of cells labeled with LysoTracker Red (LysoT Red) showed moderately enhanced colocalization with LAMP-1-positive lysosomes in STYXL1 knockdown cells (sh1: $r = 0.72 \pm 0.05$ and sh2: $r = 0.69 \pm 0.05$) compared to control cells ($r = 0.63 \pm 0.02$). Further, LysoTracker Red-positive lysosomes are dispersed throughout the STXYL1-depleted cells compared to their accumulation at the perinuclear region in control cells (Figure 1D). Quantitative analysis revealed a significant increase in the number of LysoTracker Red-positive organelles in shSTYXL1 compared to shControl cells (sh1: 393 ± 22, sh2: 364 ± 27 and C: 204 ± 21; Figure 1H). To evaluate that these acidic compartments possess proteolytic activity, we incubated the cells with a DQ-Red BSA probe and observed the processed DQ-Red fluorescence in the lysosomes.[30] Interestingly, the intensity and number of DQ-Red-positive organelles are significantly enhanced in STYXL1 knockdown compared to the control cells (sh1: 402 ± 17, sh2: 461 ± 53 and C: 212 ± 16; Figure 1D,I). Moreover, the DQ-Red-positive organelles are dispersed throughout the shSTYXL1 cells and showed increased colocalization with LAMP-1 compared to control cells (sh1: $r = 0.65 \pm 0.02$, sh2: $r = 0.64 \pm 0.02$ and C: $r = 0.55 \pm 0.04$; Figure 1D). We tested whether the dispersed lysosomes in shSTYXL1 cells will alter the degradation of cell surface cargo such as EGFR in the cells. Immunoblotting analysis showed no major change in the total EGFR protein levels in shSTYXL1 and shControl cells (Figure S1B). These studies illustrated that the depletion of STYXL1 disperses the active acidic lysosomes toward the periphery, possibly enhancing the net lysosome activity.

To test whether STYXL1 depletion alters the distribution/organization of other organelles involved in the folding and trafficking of β-GC. IFM analysis of cells stained with organelle-specific markers such as calnexin (ER), GM130 (Golgi), Rab5 (early endosomes), and LIMPII (late endosomes) showed an enhanced distribution of ER reticular network and late endosomes in shSTYXL1 cells compared to control cells. However, the shSTYXL1 cells did not show any defects in the Golgi organization but had clustered Rab5-positive early endosomes compared to shControl cells (Figure 1J). Further, the colocalization efficiency between LIMPII and LAMP-1 was not altered significantly in the cells, indicating no change in the segregation of these compartments (Figure 1K). To confirm the observed changes with ER, the shSTYXL1 cells were transfected with BIP-Myc-KDEL or KDEL-RFP to label the ER and stained the cells separately for CD63 to represent the late endosomes. Compared to control cells, shSTYXL1 cells showed an expanded KDEL-positive ER network similar to endogenous staining with calnexin (Figure S1C and quantified in Figure 1L). Additionally, shSTYXL1 cells showed enhanced peripheral distribution (>15 μm distance) of CD63-positive compartments compared to shControl cells as similar to LIMPII (Figure S1C, quantified in Figure 1M and Figure S1D). These studies demonstrated that the depletion of STYXL1 in HeLa cells affects the morphology of ER, distribution of late endosomes and lysosomes, and showed enhanced lysosomal size, acidity and cargo degradation.

2.3 | Overexpression of catalytically active STYXL1 promotes β-GC activity

We wanted to test whether the overexpression of STYXL1 can alter the lysosome enzyme activity. For this purpose, we have obtained FLAG-tagged STYXL1 (labeled as STYXL1^{WT}; Figure 2A)[10] and expressed it in HeLa cells (Figure 2B,C). Interestingly, we observed a minor reduction in β-GC activity in cells expressing STYXL1^{WT} compared to empty vector (0.84 ± 0.05 in STYXL1^{WT} and 1.00 ± 0.00 in control; Figure 2D). Furthermore, we tested the effect of a catalytically active (CA) mutant of STYXL1 (F245H and S246C) in modulating the β-GC activity (labeled STYXL1^{CA}; Figure 2A).[10] Surprisingly, the overexpression of STYXL1^{CA} mutant in HeLa cells significantly enhanced the β-GC activity (1.67 ± 0.12 in STYXL1^{CA} and 1.00 ± 0.00 in control; Figure 2B–D). In contrast to STYXL1 knockdown,

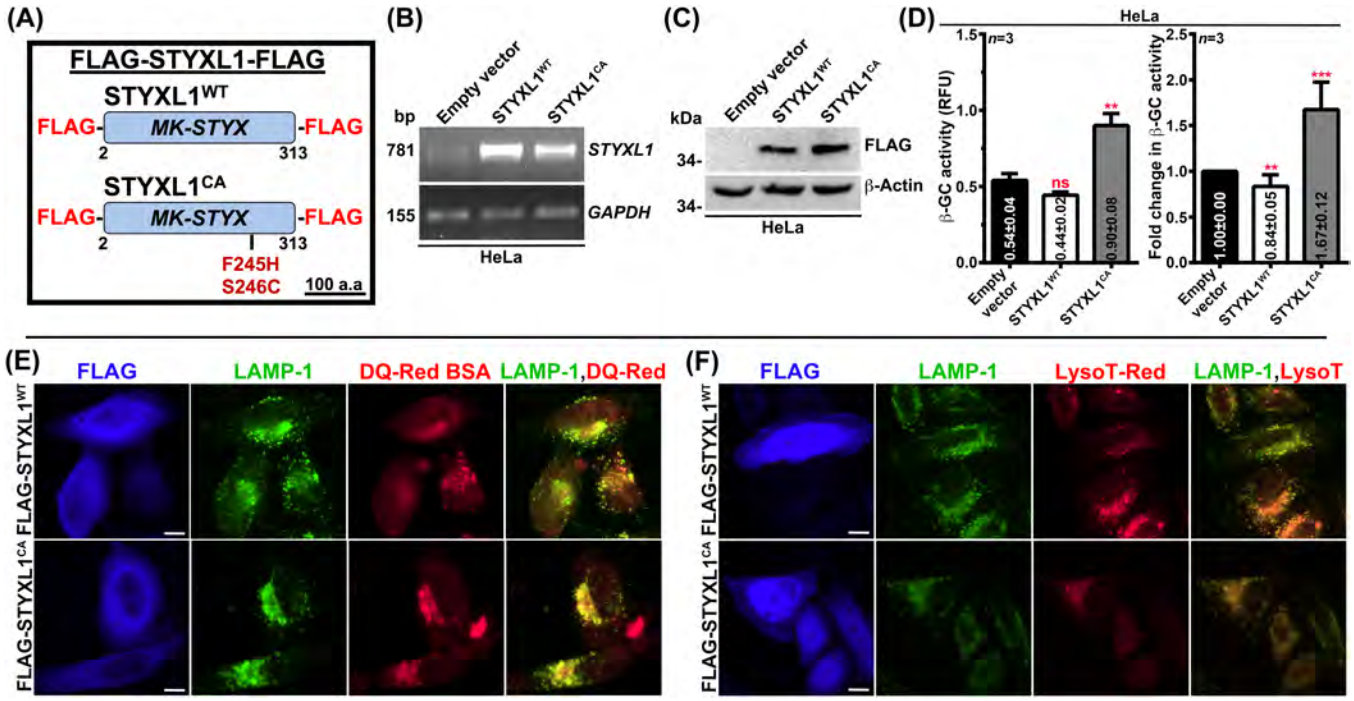

FIGURE 2 Overexpression of catalytically active STYXL1 enhances β-GC activity in HeLa cells. (A) Diagram representing the double FLAG-tagged STYTXL1 wild type (WT; STYXL1^{WT}) and constitutive active mutant (contains F245H and S246C mutations, STYXL1^{CA}). Empty vector pCDNA3 is used as a negative control to these plasmids. (B, C) Semi-quantitative RT-PCR and immunoblotting analysis of HeLa cells expressing FLAG-STYXL1-FLAG constructs to represent the transcript and protein levels. GAPDH and β-actin are used as loading control. (D) Plot representing the β-GC activity in HeLa cells expressing FLAG-STYXL1-FLAG constructs. β-GC activity in relative fluorescence units (RFUs) and fold change with respect to the control are plotted separately as mean ± s.e.m. $n = 3$. ns = not significant, $^{**}p \le 0.01$, $^{***}p \le 0.001$ and $^{****}p \le 0.0001$. (E, F) IFM analysis of HeLa cells expressing FLAG-STYXL1-FLAG constructs. Cells were stained with indicated antibodies or LysoTracker Red (F) or internalized with DQ-Red BSA (E). Scale bars, 10 μm. IFM, immunofluorescence microscopy.

STYXL1^{CA} mutant expression showed clustering of lysosomes at the perinuclear area compared to STYXL1^{WT} expressing HeLa cells (Figure 2E). Further, the lysosomes in STYXL1^{CA} mutant expressing cells display increased DQ-Red BSA processivity with reduced LysoTracker Red staining (Figure 2E,F). These results suggest that CA mutant of STYXL1 may be beneficial for improving the lysosome function; however, in in vivo this enzyme may not possess any dephosphorylation activity.[5,6,9] Overall, this data suggests that STYXL1 depletion or overexpression of its CA mutant alters the activity of β-GC in lysosomes.

2.4 | STYXL1 depletion promotes the trafficking of β-GC and its Gaucher disease mutant to lysosomes

Our experiments showed the increased β-GC activity in the STYXL1 knockdown cells was not because of a change in transcriptional or protein levels of β-GC (Figure 1C). We hypothesized that the higher enzyme activity in these cells is probably because of the enhanced trafficking of β-GC to the lysosomes. To test this hypothesis, we developed a fluorescent reporter by tagging mCherry to the C-terminus of β-GC and generated GC^{WT}-mCherry (Figure 3A).[26] It has been shown that β-GC traffics from the ER to Golgi and then to lysosomes via the endosomal pathway.[17,31] We tested the localization of GC^{WT}-mCherry reporter in HeLa cells by staining the cells with lysosomal (LAMP-1) and ER (calnexin) markers (Figure 3A and Figure S1E). As expected, the GC^{WT}-mCherry reporter majorly localized to lysosomes ($r = 0.59 \pm 0.02$ with LAMP-1; Figure 3A) and a cohort to the ER (Figure S1E) in HeLa cells. Similarly, we have generated a common Gaucher mutation N370S in GC-mCherry (referred to here as GC^{N370S}-mCherry; Figure 3B) to mimic the disease mutation. In contrast to GC^{WT}-mCherry, the mutant GC^{N370S}-mCherry reporter localized majorly to ER (Figure S1E) and a cohort to lysosomes in HeLa cells ($r = 0.36 \pm 0.04$ with LAMP-1; Figure 3B).[32,33] The knockdown of STYXL1 in HeLa cells showed enhanced localization of both GC^{WT}-mCherry and GC^{N370S}-mCherry to lysosomes (Figure 3A,B). Interestingly, the localization of mutant GC^{N370S}-mCherry reporter to the lysosomes is almost equivalent to that of GC^{WT}-mCherry (Figure 3A,B). Quantification of GC-mCherry puncta (indicative of lysosomal localization) showed a dramatic increase in the localization of mutant GC^{N370S}-mCherry reporter to the lysosomes in shSTYXL1 compared to shControl cells (Figure 3C). However, GC^{WT}-mCherry trafficking to the lysosomes was marginally increased (not significantly) in shSTYXL1 compared to shControl cells (Figure 3C). In line, the lysosomal number was also moderately changed (not significantly) in STYXL1-depleted compared to the control (Figure 3C). We tested the STYXL1^{CA} overexpression alters the trafficking of GC^{WT}-mCherry reporter to the lysosomes. Interestingly, STYXL1^{CA} mutant expression

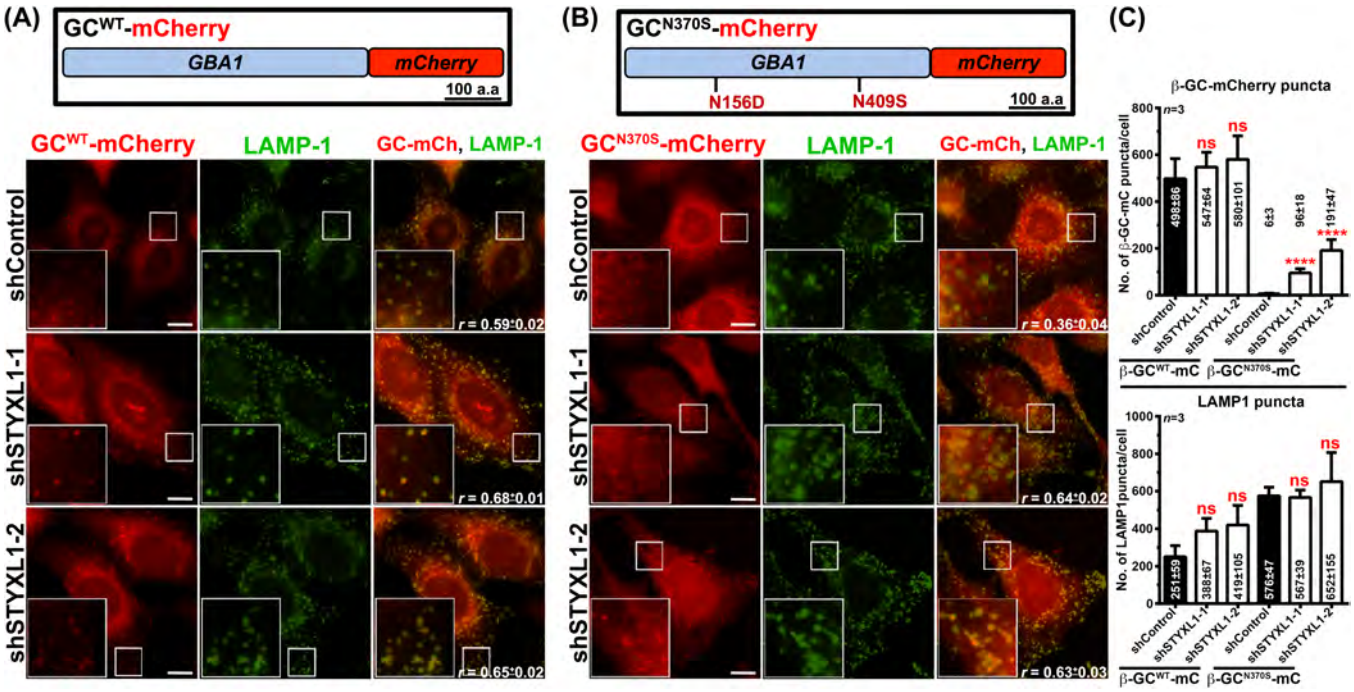

FIGURE 3 STYXL1 knockdown enhances the trafficking of wild-type (WT) or Gaucher mutant β-GC to lysosomes. (A, B) Schematic representation of β-GC$^{WT/N370S}$-mCherry reporter constructs used in this study. Scale bar, 100 a.a. Note: GC^{N370S}-mCherry construct contains an additional N156D mutation. N409S corresponds to Gaucher mutation N370S in the *GBA1* longer isoform. IFM analysis of HeLa cells expressing the β-GC^{WT}-mCherry or β-GC^{N370S}-mCherry constructs with respect to LAMP-1-postive lysosomes. The colocalization efficiency between the proteins is indicated as Pearson's coefficient (*r*) value. Insets are magnified views of the white-boxed areas. Scale bars, 10 μm. (C) Plots representing the number of β-GC-mCherry puncta/cell (top) or LAMP-1 puncta/cell (bottom). The average values in mean ± s.e.m. are indicated. $n = 3$. $^{****}p \leq 0.0001$ and ns = not significant. IFM, immunofluorescence microscopy.

in HeLa cells displayed more GC-mCherry puncta compared to STYXL1^{WT} or empty vector (GFP; Figure S1F). These studies indicate that STYXL1 depletion enhances the trafficking of Gaucher mutant β-GC^{N370S} to the lysosomes.

Next, we validated the effect of STYXL1 knockdown in restoring the β-GC activity in primary fibroblast cells of a healthy individual and derived from Gaucher patients.[26] We have obtained Gaucher disease patient Type-I (GD1) fibroblasts (GC^{N370S,84GG}, GC^{L444P}) and WT cells (from a healthy individual) from Coriell Life Sciences. The lentivirus-mediated STYXL1 depletion in primary fibroblasts marginally enhanced β-GC activity in both WT and GD1 cells (1.77 ± 0.13 in WT, 1.25 ± 0.09 in GC^{N370S,84GG} and 1.27 ± 0.11 in GC^{L444P}) compared to shControl (Figure S2A).[26] However, the fold increase in β-GC activity in the Gaucher fibroblasts was not comparable to that of WT cells (Figure S2A).[26] IFM analysis of Gaucher fibroblasts (GD1) showed enlarged and clustered (at the perinuclear area) LAMP-1-positive lysosomes compared to WT primary cells (Figure S2B).[34] The lentivirus-mediated knockdown of STYXL1 in GD1 primary fibroblasts (GC^{N370S,84GG}) caused the dispersal of lysosomes as equivalent to WT cells (Figure S2B and quantified in Figure S2C). Interestingly, the fold change in lysosomal dispersal in the primary cells was higher in 5–15 μM distance compared to HeLa cells upon the knockdown of STYXL1 in the cells (Figure S2C compared to Figure 1G). Gaucher fibroblasts having GC^{L444P} (GD1) mutation did not exhibit any enhanced lysosomal dispersion quantitatively upon STYXL1 knockdown compared to control cells (Figure S2C). Interestingly, these cells display a defect in the localization of β-GC receptor LIMPII to lysosomes compared to WT or Gaucher fibroblasts GC^{N370S,84GG} (GD1), which was mildly restored with STXYL1 depletion (Figure S2D). As similar to the lysosomes, the dispersal of LIMPII in the STYXL1-depleted primary cells (WT and GC^{N370S,84GG}) moderately increased compared to control cells (Figure S2E). Overall, these studies indicate that the depletion of STYXL1 possibly enhances the lysosome function by increasing β-GC trafficking to the dispersed lysosomes, which requires future investigation.

2.5 | STYXL1 knockdown does not alter lysosome biogenesis in the HeLa cells

We examined whether the change in lysosomal activity, size and distribution (but not the number) in shSTYXL1 is possibly because of an alteration in the transcription of lysosome biogenesis genes mediated by its transcription factors TFEB and TFE3.[35,36] Expression of TFEB-GFP showed increased nuclear localization in shSTYXL1 (76% cells in shSTYXL1-1, 60% cells in shSTYXL1-2) cells compared to shControl (12%) cells (Figure 4A). In contrast, we observed a cohort of TFE3 in the nucleus of shControl (25%) cells and was further enhanced in the

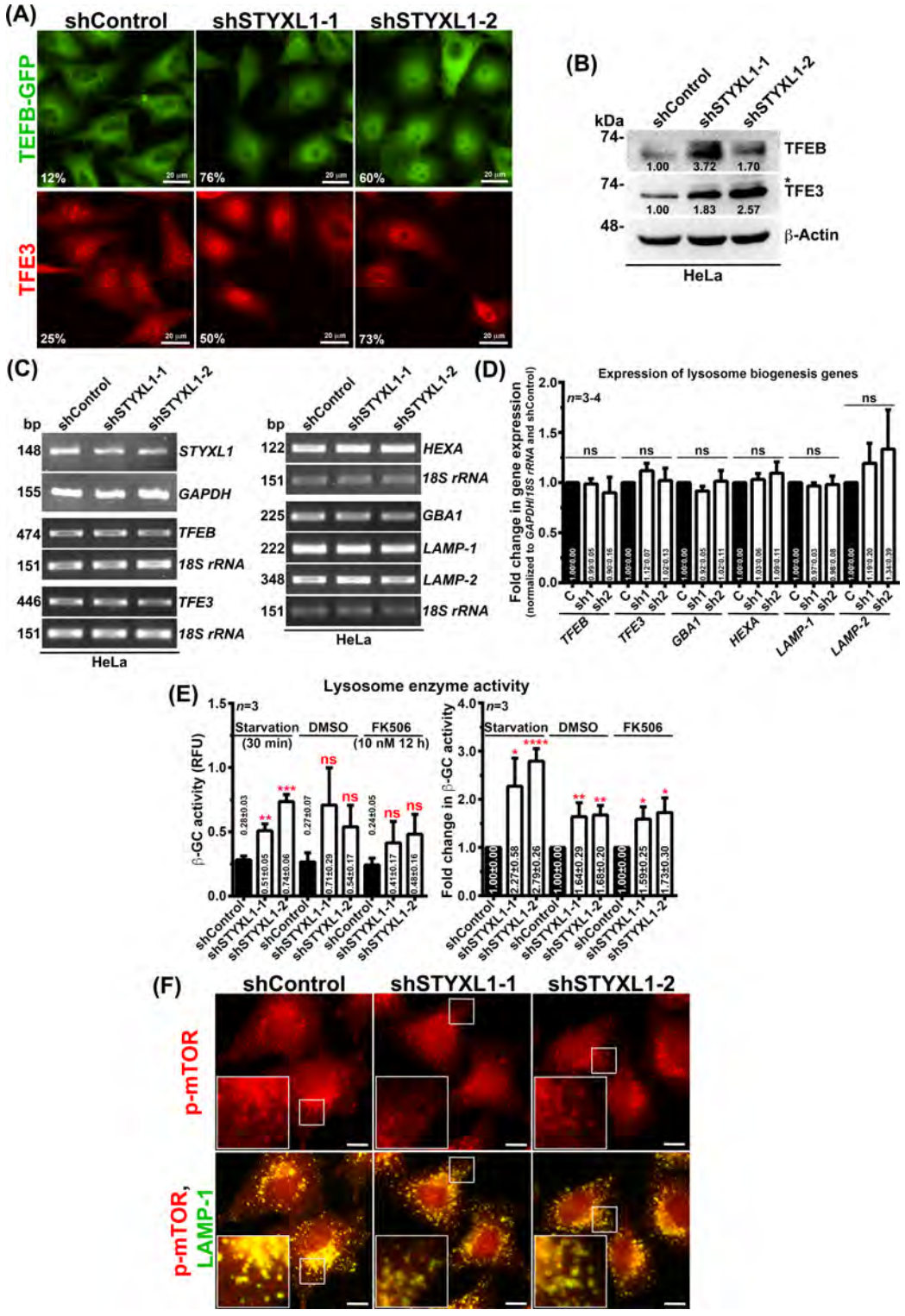

FIGURE 4 STYXL1 depletion does not alter the lysosome biogenesis but upregulates its transcription factors TFEB/TFE3 in HeLa cells. (A) IFM analysis of cells that were transfected with TFEB-GFP or stained with anti-TFE3 antibody. Visual quantification of cells showing the nuclear localization of TFEB-GFP or TFE3 is indicated separately. Scale bars, 20 μm. (B) Immunoblotting analysis of control and STYXL1-depleted HeLa cells for the expression of TFEB/TFE3. β-actin is used as a loading control. *, non-specific band developed with the antibody. The normalized fold change in the expression with respect to control is indicated on the blots. (C, D) Semi-quantitative RT-PCR analysis of control and STYXL1-depleted HeLa cells for the expression of lysosome biogenesis and its transcription factors. *GAPDH* or *18S rRNA* is used as a loading control. The normalized fold change in the transcript levels with respect to control is presented as a separate graph (D) along with the values. $n = 3$–4. (E) Plot represents the β-GC activity in RFU or fold change with respect to control cells. Cells were either starved for 30 min or treated with DMSO or FK506 (10 nM for 12 h). The average fold change values are indicated as mean ± s.e.m. $n = 3$. *$p \leq 0.05$, **$p \leq 0.01$, ***$p \leq 0.001$, ****$p \leq 0.0001$ and ns = not significant. (F) IFM analysis of control and STYXL1 knockdown HeLa cells. Cells were stained with indicated antibodies. Insets are magnified view of the white-boxed area. Scale bars, 10 μm. IFM, immunofluorescence microscopy; RFU, relative fluorescence unit.

shSTYXL1 cells (50% cells in shSTYXL1-1, 73% cells in shSTYXL1-2; Figure 4A). Next, we tested the protein levels of TFEB and TFE3 in the cells. Immunoblotting analysis showed enhanced protein levels of TFEB and TFE3 in shSTYXL1 compared to shControl cells (Figure 4B). However, the transcript levels of TFEB or TFE3 were not altered in shSTYXL1 cells compared to shControl cells (Figure 4C,D). We tested the effect of TFEB/TFE3 nuclear localization on lysosome biogenesis genes. Semi-quantitative RT-PCR showed no change in the transcript levels of several lysosomal genes such as *HEXA*, *GBA1*, *LAMP-1* and *LAMP-2* in shSTYXL1 cells compared to shControl cells (Figure 4C,D). These data suggest that STYXL1 knockdown enhances the stability and nuclear translocation of lysosome biogenesis transcription factors without inducing the transcription of downstream genes.

Studies have shown that the nuclear translocation of TFEB/TFE3 is controlled by several upstream processes such as starvation,[36,37] inactivation of calcineurin activity (using FK506)[38] or inhibition of mTOR activity.[39–41] We tested any of these conditions may promote the activity of β-GC in the lysosomes. Surprisingly, we observed that serum starvation (for 30 min) but not with FK506 (10 nM for 12 h) treatment dramatically enhanced the β-GC activity in STYXL1 knockdown compared to respective control cells (Figure 4E). Interestingly, we did not observe any change in the β-GC activity upon treatment of shControl cells with FK506 (0.24 ± 0.05 RFU) compared to DMSO (0.27 ± 0.07 RFU) or subjected to serum starvation (0.28 ± 0.03 RFU; left graph in Figure 4E), suggesting that the effects were specific to shSTYXL1 cells. Studies have shown the active form of mTOR, p-mTOR, localizes to the lysosomal membrane and phosphorylates TFEB/TFE3 depending on the nutrient status of the cells.[39–42] Therefore, we examined the localization of p-mTOR in both control and STYXL1 knockdown HeLa cells. IFM analysis revealed that the localization of p-mTOR to the lysosomes was unaffected with STYXL1 knockdown compared to control cells (Figure 4F). Further, the peripheral distribution of p-mTOR-LAMP-1 positive lysosomes was enhanced in shSTYXL1 compared to shControl cells (Figure 4F), confirming the dispersal of active lysosomes in STYXL1-depleted cells. In a nutshell, we predict that the translocation of TFEB/TFE3 to the nucleus is possibly because of upregulated unfolded protein response (UPR; see below) but not because of mTOR activity in the STYXL1 knockdown HeLa cells.

2.6 | STYXL1 depletion activates ER stress in the HeLa cells

We hypothesized that the change in ER morphology in shSTYXL1 cells is because of altered ER homeostasis, which refers to a perturbation in the fine balance between ER protein synthesis, folding, packaging and export of cargo.[43,44] This process is maintained through UPR signaling in the ER, operated through the three transmembrane proteins IRE1, ATF6 and PERK. Activation of UPR relay the stress signal by translocating the downstream transcription factors XBP1s, ATF6p and ATF4/CHOP (s = spliced and p = Golgi processed forms), respectively, to the nucleus[43] and initiating transcription of genes that restore the ER stress. Thus, we monitored the status of ER stress by examining the nuclear localization of UPR transcription factors. IFM analysis showed an increased translocation of XBP-1s, ATF6p and CHOP to the nucleus in shSTYXL1 cells compared to control cells (Figure 5A). Quantification of relative fluorescence intensity (measured by a parameter corrected total cell fluorescence, CTCF) of UPR transcription factors in the nucleus versus cytosol displayed a significant increase in the nuclear enrichment of all three factors in shSTYXL1 compared to control cells (Figure S3A). Next, we examined the transcript levels of different UPR-specific genes in shSTYXL1 and control cells (Figure S3B). Semi-quantitative PCR analysis of cells displayed increased *XBP1* transcript levels in shSTYXL1 compared to shControl cells. Further analysis revealed that XBP1 splicing was enhanced in STYXL1-depleted cells (Figure S3B). However, the downstream target genes of XBP1, such as *ERP44* but not *PDIA4* or *DNAJB9*, were moderately increased in shSTYXL1 compared to shControl cells. Interestingly, the transcripts of *ATF6* or downstream genes of PERK pathway, such as *ATF4*, *CHOP*, *HERPUD2* including *BIP* (ER chaperon), were either modestly changed or unaffected in STYXL1 knockdown cells as compared to control cells (Figure S3B). These results suggest that STYXL1 depletion results in mild upregulation of UPR pathways without inducing ER stress genes in HeLa cells. Further, we predict that the moderately enhanced UPR possibly enhances the folding/trafficking of β-GC to the lysosomes of STYXL1-depleted HeLa cells.

We tested whether UPR enhances the overall activity of β-GC activity. The STXYL1 knockdown and control cells were treated with UPR activator thapsigargin (Tg; 5 μM for 6–12 h),[45] ER stress attenuator 4-PBA (5 mM for 12–24 h)[46] or DMSO (as a control). Measurement of β-GC activity displayed an increase in shSTYXL1 cells compared to shControl in DMSO-treated cells (Figure 5B). Interestingly, the β-GC activity was not further enhanced with Tg treatment, but significantly inhibited with 4-PBA treatment in shSTYXL1 cells compared to DMSO treatment (Figure 5B). We further observed a reduction in β-GC activity in shSTYXL1 cells treated with Tg (5 μM) for 12 h compared to DMSO (Figure S3C). To know the reason for reduced β-GC activity in Tg (5 μM for 12 h) treated shSTYXL1 cells, we studied the trafficking of GC-mCherry reporter to lysosomes in HeLa cells by IFM. Surprisingly, the reporter GC-mCherry accumulated in the ER and reduced its localization to the lysosomes upon treatment with Tg for 12 h compared to DMSO (Figure S3D, quantified in Figure S3E). Additionally, β-GC activity in shSTYXL1 cells was moderately reduced upon treatment of cells with specific inhibitors of UPR pathway such as Kira6 (IRE1, 1 μM for 12 h), CeapinA-7 (ATF6, 5 μM for 12 h) and GSK2606414 (PERK, 0.1 μM for 12 h) compared to DMSO (Figure S3C). These data indicate that STXYL1 depletion enhances ER stress, which modulates the folding/trafficking of β-GC in the ER and then its activity in the lysosomes.

To further validate the observed effects are specific to STYXL1 knockdown, we traced the trafficking of GC-mCherry reporter in HeLa cells with reduced time (for 6 h) of DMSO, Tg (5 μM) or 4-PBA (5 mM) treatments. The trafficking of GC-mCherry reporter to the lysosomes was unaffected in shControl

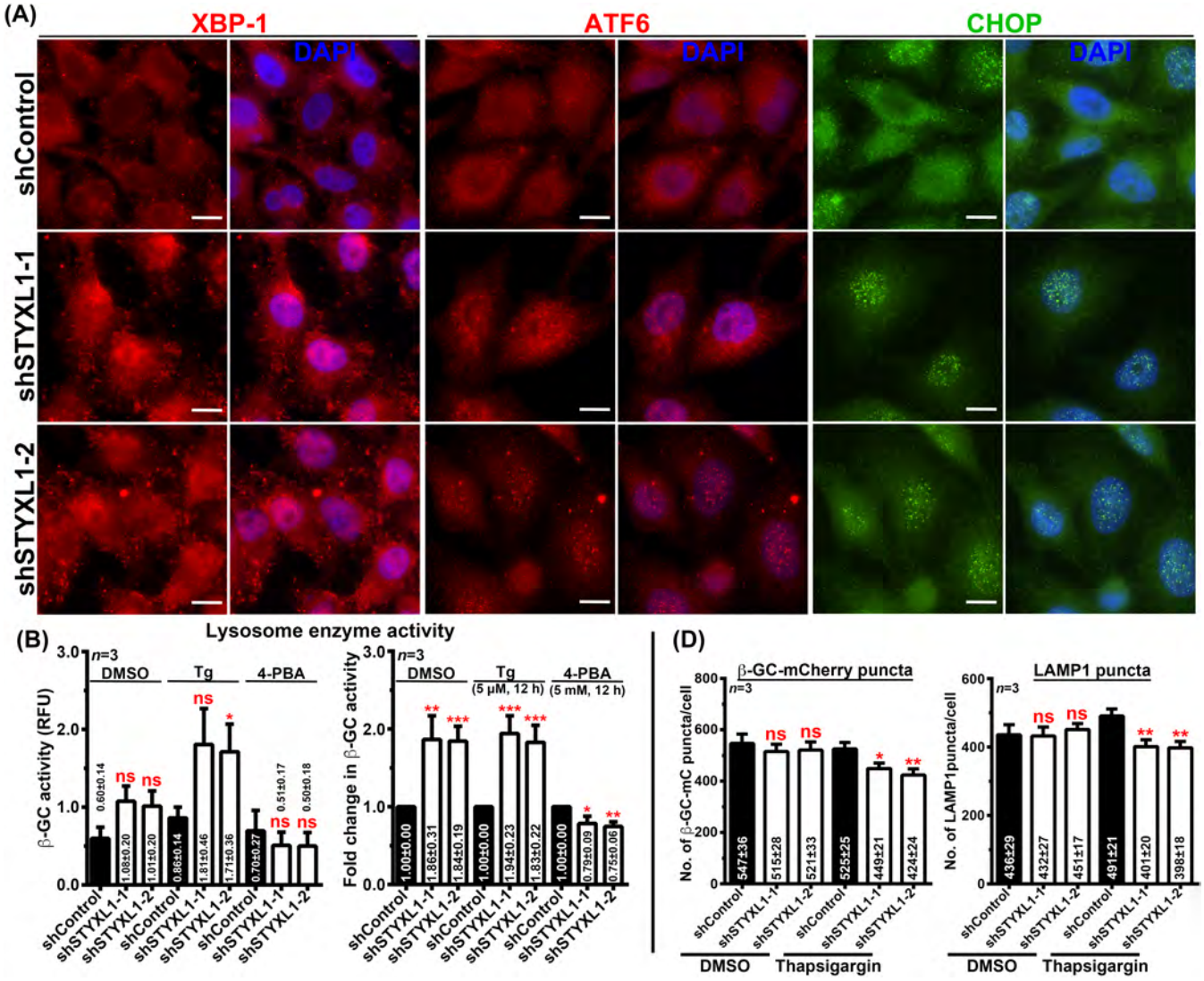

FIGURE 5 STYXL1 knockdown in HeLa cells upregulates UPR and disperses the lysosomes through its contact with ER. (A) IFM analysis of control and STYXL1 knockdown HeLa cells that were stained with indicated UPR antibodies and DAPI. (B) Plot represents the β-GC activity in control and STYXL1 knockdown HeLa cells that were treated with DMSO, thapsigargin or 4-PBA. β-GC activity in RFU and fold change with respect to the control are plotted separately as mean ± s.e.m. $n = 3$. (C) IFM analysis of GC^{WT}-mCherry stably expressing HeLa cells that were knockdown for STYXL1. Cells were treated with DMSO, thapsigargin or 4-PBA and measured the localization of GC-mCherry to lysosomes (LAMP-1). The colocalization efficiency between the GC-mCherry and LAMP-1 is indicated as Pearson's coefficient (*r*) value. (D) Plots represent the number of GC-mCherry puncta/cell or lysosomes/cell in cells treated with DMSO or thapsigargin. $n = 3$. The average values in mean ± s.e.m. are indicated. $^{*}p \leq 0.05$, $^{**}p \leq 0.01$, $^{***}p \leq 0.001$ and ns = not significant. (E) IFM analysis of control and STYXL1-depleted cells that were transfected with KDEL-RFP and then stained for LAMP1 to observe their contact. The insets are magnified view of the white boxed area. Scale bars, 10 μm. (F) Model represents the loss of pseudophosphatase STYXL1 function in mammalian cells. shRNA-mediated knockdown of STYXL1 in HeLa cells enhances the ER stress by unknown (?) mechanism, which increases the folding and trafficking of β-GC, including the Gaucher mutant (upward red arrow) to lysosomes. This process improves the function of the lysosomes in addition to their spread along with ER. Further, upregulated ER stress activates the lysosomes biogenesis transcription factors (TFEB/TFE3) without changing the gene expression, possibly contributing to the lysosome function (dotted arrow). ER, endoplasmic reticulum; IFM, immunofluorescence microscopy; UPR, unfolded protein response; WT, wild-type.

cells after the treatment with Tg or 4-PBA for 6 h in comparison with DMSO (Figure 5C). As expected, the trafficking of GC-mCherry reporter to the lysosomes was increased in shSTYXL1 cells and was reduced upon treatment of the cells with Tg or 4-PBA for 6 h (Figure 5C and quantified in Figure 5D). These studies suggest that the knockdown of STXYL1 promotes the trafficking of β-GC to the lysosomes.

To understand the possible mechanism for the dispersal of lysosomes in STYXL1 cells, we examined the association of dispersed lysosomes with expanded ER.[47] The cells depleted with STYXL1 showed expanded ER (marked by KDEL-RFP) and dispersed lysosomes (LAMP-1) compared to control cells (Figure 5E). Interestingly, the association of LAMP-1-positive lysosomes with ER was also enhanced in shSTYXL1 cells compared to shControl cells (Figure 5E).

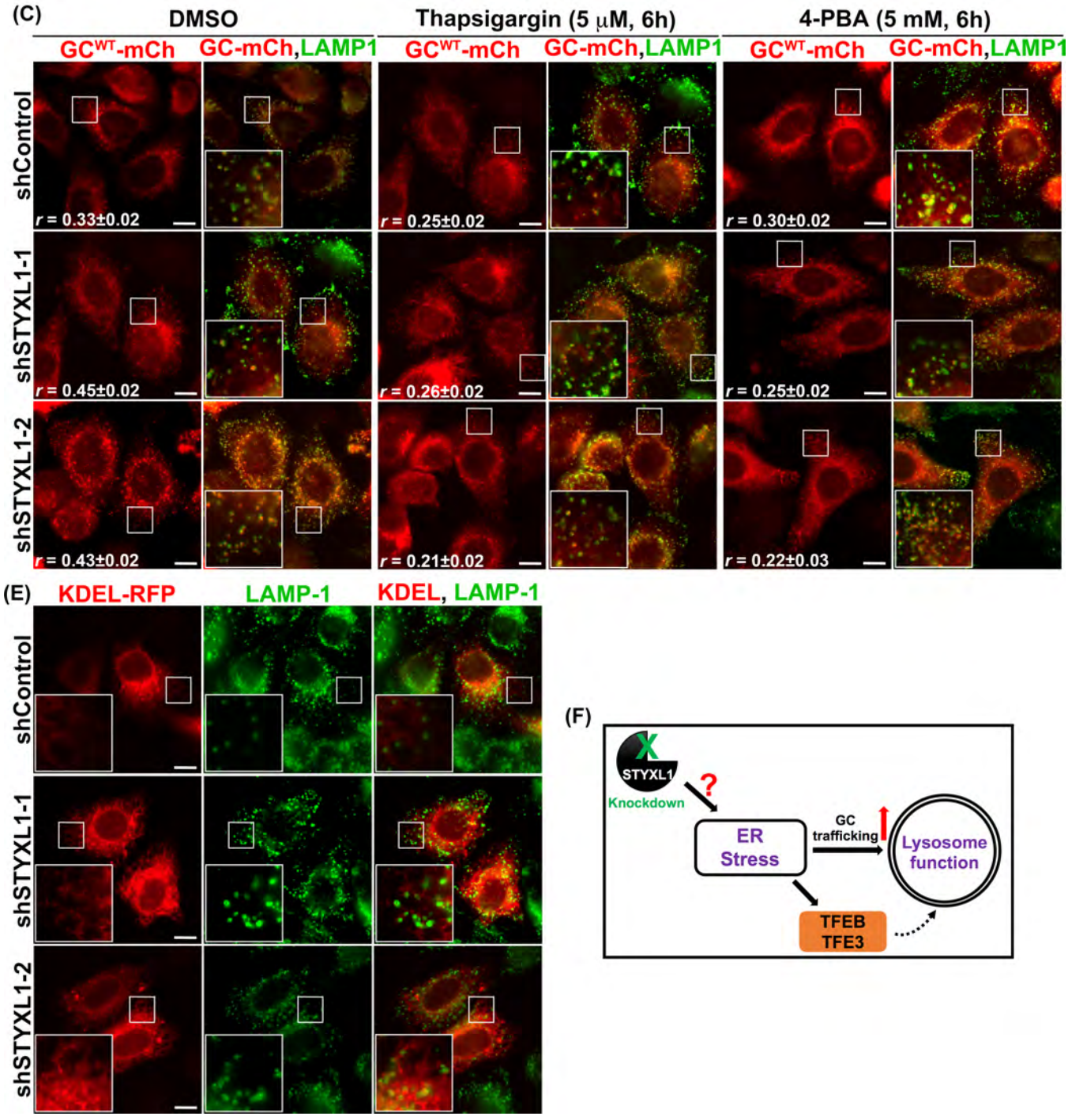

FIGURE 5 (Continued)

Next, we tested whether the ER stress can cause the enhanced association of ER-lysosome contacts in HeLa cells. Treatment of cells with tunicamycin (10 μM) for 6 h displayed the enhanced distribution of lysosomes as well as expanded ER along with increased ER-lysosomal contacts compared to DMSO (Figure S3F). These results suggest that STYXL1 knockdown in HeLa cells may result in ER stress, which possibly enhances the trafficking of β-GC to the lysosomes and disperse these organelles through expanded ER.

3 | DISCUSSION

Gaucher disease is caused because of decreased β-GC activity in the lysosomes of mammalian cells. The mutations contributing to Gaucher disease are majorly eliminated from ER because of defective folding and export to Golgi.[23–25] Interestingly, the majority of these mutant proteins possess enzyme activity and are able to hydrolyze the substrate glucosylceramide to glucose and ceramide, although at a slower rate than

WT.[27,33,48] The accumulation of glucosylceramide in the lysosomes of Gaucher patients affects many cellular metabolic and signaling pathways.[34,49,50] The lipid-laden macrophages in the Gaucher patients activate cytokine, and related pathways result in inflammation[51] that causes spleen and liver enlargement.[52] Several treatments are available for Gaucher disease; however, all are specific to non-neuropathic forms of the disease. In recent times, several small molecular-based therapies are also proposed, which are under clinical trials.[18,53] In this study, we attempted to illustrate a role for pseudophosphatase STYXL1, identified as a hit in an RNAi screen to improve the activity of β-GC enzyme in the lysosome.[26] We studied the effect of STYXL1 knockdown on the folding and trafficking of β-GC from ER to Golgi and its activity in the lysosomes. These studies demonstrated that the depletion of STYXL1 enhances the trafficking of β-GC and its lysosomal activity. Further, STXYL1 knockdown cells display expanded ER and increased lysosome size, acidity, proteolytically activity and cellular distribution. Additionally, STYXL1 depletion generates moderate ER stress, which possibly is responsible for lysosomal dispersal through ER-lysosome contacts. Our preliminary data showed that STYXL1 depletion marginally increased the β-GC activity[26] and lysosomal distribution in one set of Gaucher patient fibroblasts. However, the observed mild changes in Gaucher patient cells are unlikely to be relevant in a clinical/translation setting.

Phosphatases are an important class of cellular enzymes that modulate cellular trafficking and signaling pathways by dephosphorylating different substrates (proteins or lipids).[1–3] Pseudophosphatases are catalytically dead enzymes whose role in regulating cellular pathways recently came into the light.[5–7] Pseudophosphatases can stimulate the function of phosphatases by acting as a cofactor or inhibit their function by dimerization. Mutations associated with pseudophosphatases are reported to cause different diseases, explaining their role in cell physiology.[7] STYXL1 is reported as a pseudophosphatase[10] and its function has been described in a few cellular processes in different cell types.[10,12,13,15,16,54–56] However, its role in lysosome function or organelle dispersion has not been reported. We found a unique negative function of STXYL1 in altering the trafficking of lysosomal enzyme β-GC. Our study also identified that the loss of STYXL1 protein results in moderately enhanced UPR and ER expansion (Figures 1 and 5). Interestingly, we observed the activation of all three branches of UPR reflecting a general ER stress in the STYXL1-depleted HeLa cells, which possibly is responsible for enhanced trafficking of lysosome hydrolases from ER to Golgi (Figure 5F). Further, starvation of STYXL1 knockdown cells but not the treatment with an ER stress activator such as thapsigargin enhanced the β-GC activity. In contrast, inhibition of ER stress through 4-PBA reduced the β-GC activity to basal level in STYXL1-depleted cells (Figure 5). We predict that the enhanced ER stress in shSTYXL1 cells possibly caused the nuclear translocation of TFEB and TFE3 but did not induce the lysosome biogenesis genes (Figures 4 and 5F). Expression of CA mutant of STYXL1 also enhanced the lysosome activity in the HeLa cells (Figure 2). These studies indicate that pseudophosphatase STYXL1 acts as a negative regulator of ER stress or lysosome activity in vivo (Figure 5F). However, the loss of function or mutation causing restoration of phosphatase activity (similar to STYXL1^{CA}) in STYXL1 may have a large clinical impact in the field of lysosome storage diseases such as Gaucher disease. Here, we only showed the loss of function through shRNA-mediate knockdown in HeLa cells, which enhanced the distribution of lysosomes and their activity through ER-lysosome contacts. Additionally, Gaucher patient fibroblasts moderately restored the lysosome activity and their cellular distribution, indicating an indirect role of this pseudophosphatase in altering the trafficking of acid hydrolases (including Gaucher mutants) to the lysosomes. In future, identifying a small-molecular inhibitor against STYXL1 possibly acts as a therapeutic agent to alter the status of Gaucher disease. This process has several advances: (1) although cells displayed nuclear translocation of CHOP upon STYXL1 depletion but did not induce apoptosis; (2) small molecules can cure the neuropathic form of Gaucher disease; and (3) this process possibly cures other forms of LSDs. However, these possibilities require future investigation.

The distribution of organelles plays a vital role in their function, especially lysosomes. Lysosomes appeared as clusters at the perinuclear area in the majority of the cells, such as HeLa. The distribution of lysosomes to the periphery alters their activity.[28,29] Interestingly, STYXL1 depletion enhanced the dispersion of ER, late endosomes and lysosomes. Moreover, the peripherally distributed lysosomes are acidic and proteolytically active (Figure 1), and showed more contact with ER (Figure 5) in STYXL1-depleted cells, suggesting an indirect role of STYXL1 in regulating the distribution of cohort of eukaryotic organelles.[11] It is unknown how the lysosome distribution is affected in Gaucher disease. Our studies showed dispersal of lysosomes promoted their activity, which may reduce the accumulation of storage in the cells. We predict that this method may delay the progression of Gaucher disease, especially beneficial for neuropathic forms. Moreover, we also speculate that the dispersion of the organelles in shSTYXL1 cells may be because of an alteration in post-translational modification of microtubules since STYXL1 overexpression enhances detyrosinization and acetylation of microtubules.[16] Inline, the detyrosinization of microtubules is shown to reduce the lysosomes' motility.[57] Therefore, STYXL1 depletion possibly affects the post-translation modification of microtubules, which may alter the ER distribution and lysosome positioning. Mitochondrial dysfunction has been observed in several Gaucher disease models.[58–61] Interestingly, STYXL1 knockdown prevents the cytochrome C release from mitochondria and blocks apoptosis under various cellular stress conditions.[12] Further, STYXL1 physically interacts with mitochondrial phosphatase PTPMT1 and negatively regulates its function during mitochondrial-dependent cell death.[13] Based on these studies, we also predict that the change in UPR status may alter the mitochondrial dynamics in shSTYXL1 cells, which requires further studies. Nevertheless, identifying a small molecule to inhibit the pseudophosphatase STYXL1 function beneficial for curing Gaucher disease and other forms of LSD.

4 | MATERIALS AND METHODS

4.1 | Reagents and antibodies

All chemicals and reagents were purchased either from Sigma-Aldrich (Merck) or Thermo Fisher Scientific (Invitrogen). 4-PBA, 4-methylumbelliferyl β-D-glucopyranoside (MUD), ceapinA-7, FK506, GSK2606414, kira6, puromycin, resazurin, thapsigargin and tunicamycin were purchased from Sigma-Aldrich (Merck).

Conduritol B epoxide (CBE) was procured from Tocris Bioscience. LysoTracker Red DND-99 (L7528) and DQ-Red BSA (D12051) were obtained from Thermo Fisher Scientific (Invitrogen). The following commercial polyclonal and monoclonal antisera were used (m, mouse; h, human and r, rat proteins): anti-LIMPII (ab16522) was from Abcam; anti-Calnexin (610523) and anti-GM130 (610822) were from BD Biosciences; anti-CHOP (2895), anti-hLAMP-1 (9091), anti-Rab5 (3547) and anti-TFEB (4240) were from Cell Signalling Technology; anti-hCD63 (H5C6) and anti-hLAMP-1 (H4A3) were from Developmental Studies Hybridoma Bank; anti-ATF6α (sc-22 799) and anti-XBP-1 (sc-7160) were from Santa Cruz Biotechnology; anti-β-actin (A5441), anti-FLAG M2 (F1804), anti-hGlucocerebrosidase (GBA/GC; G4171) and anti-TFE3 (HPA023881) from Sigma-Aldrich (Merck). All secondary antibodies were either from Invitrogen or Jackson ImmunoResearch.

4.2 | Plasmids and shRNAs

$GC^{WT/N370S/L444P}$-VSVG-pCDNA3.1+ constructs were a kind gift from Jeffery Kelly, Scripps Institute.[48] FLAG-$STYXL^{WT}$-FLAG and FLAG-$STYXL^{F245H,S246C}$-FLAG constructs were a kind gift from Shanta D. Hinton, College of William and Mary.[10] KDEL-RFP plasmid was a kind gift from Nagaraj Balasubramanian, IISER Pune.[62] pMD2.G (VSV-G lentiviral envelope vector, 12259), psPAX2 (lentiviral packaging vector, 12260) and BiP-Myc-KDEL (27164) were obtained from Addgene. TFEB-GFP[63] has been described previously.

GFP-$STYXL1^{WT/CA}$ plasmids were made by subcloning the $STYXL1^{WT/CA}$ inserts from their respective FLAG-tagged vectors into pEGCP-C1 (Clontech). $GC^{WT/N370S/L444P}$-mCherry-pCDNA3.1+ constructs were prepared by PCR amplifying the genes from $GC^{WT/N370S/L444P}$-VSVG-pCDNA3.1+ vectors and then cloned as in-frame fusion to mCherry in mCherry-pCDNA3.1+ vector (available in the lab). $GC^{WT/N370S/L444P}$-mCherry-pLVX-puro constructs were made by subcloning the $GC^{WT/N370S/L444P}$ -mCherry inserts from their respective pCDNA3.1+ vectors into pLVX-puro (Clontech). All constructs were sequenced before use. We found an additional N156D mutation in the GC^{N370S}-mCherry constructs in addition to N370S (Figure 3). Note that N370S in GC^{N370S}-mCherry corresponds to N409S mutation in the longer isoform-1 of *GBA* (*GBA1*). Similarly, the mutation L483P in GC^{L444P}-mCherry constructs represents L444P of *GBA1*.[21]

shRNAs against STYXL1 gene (shSTYXL1-1: 5′-GCATAGTAACGAGCAGACCTT-3′; shSTYXL1-2: 5′-GCTTTACAACATCCTGAATCA-3′) were from a focused set of phosphatases in the human TRC shRNA library, purchased from Sigma-Aldrich (Catalog no. SH0411). pLKO.1-puro Non-mammalian shRNA (referred to here as shControl, SHC002) was used as a control in all the experiments.

4.3 | Cell culture, transfection and lentiviral transduction

HeLa and HEK293T were procured from ATCC and maintained in DMEM (Invitrogen) supplemented with 10% FBS (Biowest), 1% L-glutamine (Invitrogen) and 1% penicillin–streptomycin (Pen-Strep, Invitrogen) antibiotics at 37°C with 10% CO_2 in a humified cell culture chamber. Human primary fibroblasts were procured from Coriell Cell Repositories and maintained in MEM (GIBCO) medium supplemented with 10% FBS (Biowest) and 1% Pen-Strep antibiotics (Invitrogen) at 37°C with 10% CO_2 in a humified cell culture chamber. The following primary cells were used in this study. WT: apparently healthy individual from non-fetal tissue, skin origin (GM00498); $GC^{N370S,84GG}$: non-neuropathic Gaucher disease, Type I (GD1), skin origin (GM00372) and GC^{L444P}: non-neuropathic GD1, unknown origin (GM10915).[26]

Transient transfection of the cells with plasmids was performed post-incubation of the cells in OPTI-MEM (Invitrogen) for 30 min and followed the manufacturer's protocol of Lipofectamine 2000 (Invitrogen). For shRNA-mediated knockdown, cells were seeded at a confluency of 80% in a well of 24-well plate. Post 12 h of seeding, cells were transfected with a cocktail containing 500 ng of STYXL1 shRNA or shControl and 0.75 μL Lipofectamine 2000 in OPTI-MEM. Cells were supplemented with a complete medium after 5 h of transfection. Post 48 h of transfection, the cells were used it for biochemical assay or IFM. In certain experiments, the shRNA-mediated knockdown cells were further transfected with plasmids using Lipofectamine 2000 post 24 h of shRNA transfection. The primary cells were transduced with lentivirus encoding GC-mCherry expression vectors or shRNAs using a protocol described previously.[64] In Figure 4E, the cells were subjected to 30 min starvation in plain DMEM medium (without FBS). In Figures 4 and 5 and Figure S3, the cells were treated with different drugs as follows: 4-PBA (5 mM for 6–12 h), FK506 (10 nM for 12 h), thapsigargin (Tg, 5 μM for 6–12 h), tunicamycin (Tu, 10 μM for 6 h), kira6 (1 μM for 12 h), ceapinA-7 (5 μM for 12 h) and GSK2606414 (0.1 μM for 12 h). As a control, DMSO was used during these treatments.

4.4 | LysoTracker Red uptake and DQ-Red BSA trafficking assays

LysoTracker Red uptake was carried out by incubating the cells on a coverslip with a medium containing 100 nM of LysoTracker Red for 1 h at 37°C and then fixed with 4% paraformaldehyde. Similarly, cells were incubated in a medium containing 10 μg/mL DQ-Red BSA for 12 h at 37°C and then chased in a plain medium for 6 h followed by fixing the cells with 3% paraformaldehyde. Further, cells were immunostained with anti-LAMP-1 antibody and then imaged. The number of LysoTracker Red/DQ-Red -positive puncta was quantified using ImageJ. Briefly, the images were converted into binary format, followed by applying a common threshold to all images. Further, overlapping objects in the binary images were separated using the Watershed parameter and then quantified the number of puncta by choosing to analyze particle parameters without placing any limit on size and circularity.

4.5 | IFM and image analysis

Immunostaining of cells with respective primary and secondary antibodies was carried out post-fixation of cells with 3% formaldehyde on

the coverslips as described previously.[65] IFM of cells was performed on an Olympus IX81 motorized inverted fluorescence microscope equipped with a CoolSNAP HQ2 (Photometrics) CCD camera using a 60× (oil) U Plan super apochromatic objective. Deconvolution of images was carried out using the cellSens Dimension package with the 5D module (Olympus) and analyzed.[65] Briefly, cells were imaged for 10–12 z-stacks with a z-step size of 0.2 μm. In Figure 1D, the z-stacks were subjected to constrained iterative deconvolution (1 or 2 iterations) using the cellSens Dimension package. Otherwise, undeconvolved z-stack images were converted to maximum intensity projection and used for further use. Final images were converted into TIFF format and then assembled using Adobe Photoshop. The Pearson's correlation (*r*) value between two colors was estimated using cellSens Dimension software. Multiple ROIs (regions of interest) in the cytosol (excluding perinuclear area) of maximum intensity projection of undeconvolved z-stack images were selected for the analysis and then measured (as mean ± s.e.m.) the average *r* value from 20 to 30 cells. The localization of the transcription factor to the nucleus (in reference to DAPI staining) was measured as CTCF (corrected total cell fluorescence) ratio between the nucleus and cytoplasm, measured separately. The averaged CTCF ratio from 10 to 20 cells was calculated using the below formula and then plotted. CTCF (in arbitrary units, A.U.) = Integrated density of the cell or nucleus − (area of the selected cell or nuclear × mean fluorescence intensity of the background). The mean fluorescence intensity of the images was quantified using ImageJ.

4.6 | Quantification of IFM

4.6.1 | Organelle number

The number of lysosomes or GC-mCherry puncta was quantified using Fiji with ComDet v.0.5.5 plugin. Average number of lysosomes or GC-mCherry puncta/cell was plotted.

4.6.2 | Lysosome size

The size of the lysosomes was calculated using Fiji software. The images were converted into 8 bit followed by applying the auto-threshold to all binary images. The particle (lysosomes) size was measured using Analyze particles option. The size of lysosome (μm^2) in each condition was plotted.

4.6.3 | ER dispersion

The percentage area occupied by ER sheet was calculated using Fiji software. The total area spread by ER (sheet and tubular forms) and ER sheet alone within the cell was calculated separately. The ER dispersion = (Total area occupied by ER sheet/Total area of the cell)*100.

4.6.4 | LAMP1/LIMPII/CD63 distribution

The distribution of different organelles was calculated using Fiji with radial intensity profile plugin as described previously.[66] Each cell was divided into three areas (0–5, 5–15 and >15 μm) from the center of the cell and determine the radial profile intensity. The data was plotted after normalizing the radial profile intensities in the areas 5–15 and >15 μm with 0–5 μm in each cell. The distribution of the organelles in 5–15 and >15 μm was plotted separately.

4.7 | β-glucocerebrosidase (GC) activity and cell viability assays

Cells were plated in triplicate wells of 96-well clear flat-bottom black plate (Corning) at 70%–80% confluency. The cell viability[63] and lysosomal β-glucosidase activity[27] assays were performed as follows. Cells were added with 1 mg/mL of resazurin in the growth medium and then incubated at 37°C for 3–4 h. The fluorescence intensity (excitation: 530 nm and emission: 590 nm) was measured using a Tecan multi-mode plate reader (Infinite F200 Pro). The obtained A.U. value was used to normalize the β-GC activity, measured in the same well. Further, the cells were washed twice with 1× PBS post resazurin assay and then incubated at 37°C with 50 μL of 3 mM MUD (4-methyl umbelliferyl-β-D-glucopyranoside, made in 0.2 M sodium acetate buffer pH 4.2). The assay was stopped with 150 μL of 0.2 M glycine buffer pH 10.8 after 150 min (2.5 h). The liberated 4-methylumbelliferone (excitation: 365 nm and emission: 445 nm) fluorescence intensity was measured using a Tecan multi-mode plate reader. Finally, the lysosomal enzyme activity (in A.U.) per well was normalized with respective cell viability values (referred to as relative fluorescence units, RFU). The fold change in GC activity in shSTYXL1 with shControl cells was calculated. The data representing the β-GC activity in RFU and fold change with respect to control were plotted separately. Note that the β-GC activity in the primary human fibroblasts was stopped post 60 min of incubation. In certain experiments, cells in additional triplicate wells were added with 600 μM of CBE (conduritol B epoxide) along with MUD. The obtained values with CBE are considered as β-GC (*GBA1*) specific activity but not because of non-lysosomal glucocerebrosidase activity (contributed by *GBA2*, *GBA3* genes and other enzymes). Interestingly, the presence or absence of CBE did not show any difference in β-GC activity in HeLa cells (data not shown), indicating the measured activity is specific to β-GC.

4.8 | Transcript-level analysis of genes by semi-quantitative or quantitative PCR

RNA isolation from the cells was performed by using GeneJET RNA purification kit (Thermo Fisher Scientific) in the presence of β-mercaptoethanol followed by estimating the concentration using NanoDrop 2000C spectrophotometer (Thermo Fisher Scientific). The cDNA

was synthesized from RNA using a cDNA synthesis kit (Fermantas). The transcripts were amplified in a Bio-Rad S1000 Thermal Cycler using an equal amount of cDNA from each condition and the gene-specific primers. The primers used in this study are listed in Table S1. As a control, *18S rRNA* or *β-ACTIN* or *GAPDH* was used. The gels were imaged in a Bio-Rad Molecular Imager ChemiDoc XRS+ imaging system using Image Lab 4.1 software. DNA band intensities were quantified and then normalized with a loading control. The fold change in values with respect to control is indicated on the gels or plotted separately.

4.9 | Immunoblotting

Cells were lysed in RIPA buffer and then subjected to immunoblotting analysis as described previously.[64] Immunoblots were developed with Clarity Western ECL substrate (Bio-Rad) and then imaged in a Bio-Rad Molecular Imager ChemiDoc XRS+ imaging system using Image Lab 4.1 software. Protein band intensities were quantified and then normalized with a loading control. The fold change in values with respect to control is indicated in the figure.

4.10 | Statistical analysis

GraphPad Prism 6.0 software was used to calculate the statistical analysis of all samples. The statistical significance was determined by unpaired Student's *t* test and variance analysis. ns = not significant, $^{*}p \le 0.05$, $^{**}p \le 0.01$, $^{***}p \le 0.001$ and $^{****}p \le 0.0001$.

AUTHOR CONTRIBUTIONS

Saloni Patel performed all the initial experiments of this study. Anshul Milap Bhatt conducted all the experiments required for the revision of this MS and quantification of the data. Priyanka Bhansali supported the study by quantifying the IFM of lysosomal transcription factors. Subba Rao Gangi Setty designed, oversaw the entire project, coordinated and discussed the work with co-authors and wrote the manuscript.

ACKNOWLEDGMENTS

The authors thank Shanta D. Hinton for the generous gift of the MK-STYX plasmids. The authors thank Jeffery Kelly, Dan Garza and Ting-Wei Mu for sharing the GC-VSVG plasmids and initial technical support for the GC activity assay. The authors thank Anup, Madhavi Latha and Darpan for their technical help. This work was supported by the Department of Biotechnology (BT/PR4982/AGR/36/718/2012 and BT/PR32489/BRB/10/1786/2019), Science and Engineering Research Board (CRG/2019/000281), National Bioscience Award (BT/HRD-NBA-NWB/38/2019-20), and The Wellcome Trust DBT India Alliance (500122/Z/09/Z). AMB and PB were supported by DBT-JRF (DBT/2015/IISc/NJ-02 and DBT/2016/IISc/717, respectively).

CONFLICT OF INTEREST STATEMENT

The authors declare no conflict of interest.

DATA AVAILABILITY STATEMENT

Data available on request from the authors.

ORCID

Subba Rao Gangi Setty https://orcid.org/0000-0003-4035-2900

REFERENCES

1. Mustelin T. A brief introduction to the protein phosphatase families. *Methods Mol Biol*. 2007;365:9-22.
2. Sacco F, Perfetto L, Castagnoli L, Cesareni G. The human phosphatase interactome: an intricate family portrait. *FEBS Lett*. 2012;586(17):2732-2739.
3. Liberti S, Sacco F, Calderone A, et al. HuPho: the human phosphatase portal. *FEBS J*. 2013;280(2):379-387.
4. Reiterer V, Eyers PA, Farhan H. Day of the dead: pseudokinases and pseudophosphatases in physiology and disease. *Trends Cell Biol*. 2014;24(9):489-505.
5. Hinton SD. The role of pseudophosphatases as signaling regulators. *Biochim Biophys Acta Mol Cell Res*. 2019;1866(1):167-174.
6. Reiterer V, Pawlowski K, Desrochers G, Pause A, Sharpe HJ, Farhan H. The dead phosphatases society: a review of the emerging roles of pseudophosphatases. *FEBS J*. 2020;287(19):4198-4220.
7. Mattei AM, Smailys JD, Hepworth EMW, Hinton SD. The roles of pseudophosphatases in disease. *Int J Mol Sci*. 2021;22(13):6924.
8. Hinton SD. Analyzing pseudophosphatase function. *Methods Mol Biol*. 2016;1447:139-153.
9. Hinton SD. Pseudophosphatase MK-STYX: the atypical member of the MAP kinase phosphatases. *FEBS J*. 2020;287(19):4221-4231.
10. Hinton SD, Myers MP, Roggero VR, Allison LA, Tonks NK. The pseudophosphatase MK-STYX interacts with G3BP and decreases stress granule formation. *Biochem J*. 2010;427(3):349-357.
11. Reiterer V, Fey D, Kolch W, Kholodenko BN, Farhan H. Pseudophosphatase STYX modulates cell-fate decisions and cell migration by spatiotemporal regulation of ERK1/2. *Proc Natl Acad Sci U S A*. 2013;110(31):E2934-E2943.
12. Niemi NM, Lanning NJ, Klomp JA, et al. MK-STYX, a catalytically inactive phosphatase regulating mitochondrially dependent apoptosis. *Mol Cell Biol*. 2011;31(7):1357-1368.
13. Niemi NM, Sacoman JL, Westrate LM, et al. The pseudophosphatase MK-STYX physically and genetically interacts with the mitochondrial phosphatase PTPMT1. *PLoS One*. 2014;9(4):e93896.
14. Reiterer V, Figueras-Puig C, Le Guerroue F, et al. The pseudophosphatase STYX targets the F-box of FBXW7 and inhibits SCFFBXW7 function. *EMBO J*. 2017;36(3):260-273.
15. Flowers BM, Rusnak LE, Wong KE, et al. The pseudophosphatase MK-STYX induces neurite-like outgrowths in PC12 cells. *PLoS One*. 2014;9(12):e114535.
16. Cao Y, Banks DA, Mattei AM, et al. Pseudophosphatase MK-STYX alters histone deacetylase 6 cytoplasmic localization, decreases its phosphorylation, and increases detyrosination of tubulin. *Int J Mol Sci*. 2019;20(6):1455.
17. Ballabio A, Bonifacino JS. Lysosomes as dynamic regulators of cell and organismal homeostasis. *Nat Rev Mol Cell Biol*. 2020;21(2):101-118.
18. Platt FM, d'Azzo A, Davidson BL, Neufeld EF, Tifft CJ. Lysosomal storage diseases. *Nat Rev Dis Primers*. 2018;4(1):27.
19. Horowitz M, Wilder S, Horowitz Z, Reiner O, Gelbart T, Beutler E. The human glucocerebrosidase gene and pseudogene: structure and evolution. *Genomics*. 1989;4(1):87-96.
20. Kretz KA, Carson GS, Morimoto S, Kishimoto Y, Fluharty AL, O'Brien JS. Characterization of a mutation in a family with saposin B deficiency: a glycosylation site defect. *Proc Natl Acad Sci U S A*. 1990;87(7):2541-2544.
21. Hruska KS, LaMarca ME, Scott CR, Sidransky E. Gaucher disease: mutation and polymorphism spectrum in the glucocerebrosidase gene (GBA). *Hum Mutat*. 2008;29(5):567-583.

22. Stirnemann J, Belmatoug N, Camou F, et al. A review of Gaucher disease pathophysiology, clinical presentation and treatments. *Int J Mol Sci*. 2017;18(2):441.
23. Ron I, Horowitz M. ER retention and degradation as the molecular basis underlying Gaucher disease heterogeneity. *Hum Mol Genet*. 2005;14(16):2387-2398.
24. Tan YL, Genereux JC, Pankow S, Aerts JM, Yates JR 3rd, Kelly JW. ERdj3 is an endoplasmic reticulum degradation factor for mutant glucocerebrosidase variants linked to Gaucher's disease. *Chem Biol*. 2014;21(8):967-976.
25. Yang C, Wang H, Zhu D, et al. Mutant glucocerebrosidase in Gaucher disease recruits Hsp27 to the Hsp90 chaperone complex for proteasomal degradation. *Proc Natl Acad Sci U S A*. 2015;112(4):1137-1142.
26. Patel S, Radhakrishnan D, Kumari D, Bhansali P, Setty SRG. Restoration of β-GC trafficking improves the lysosome function in Gaucher's disease. *bioRxiv*. 2022. doi:10.1101/2022.06.23.497394
27. Sawkar AR, Cheng WC, Beutler E, Wong CH, Balch WE, Kelly JW. Chemical chaperones increase the cellular activity of N370S beta -glucosidase: a therapeutic strategy for Gaucher disease. *Proc Natl Acad Sci U S A*. 2002;99(24):15428-15433.
28. Bagshaw RD, Callahan JW, Mahuran DJ. The Arf-family protein, Arl8b, is involved in the spatial distribution of lysosomes. *Biochem Biophys Res Commun*. 2006;344(4):1186-1191.
29. Johnson DE, Ostrowski P, Jaumouille V, Grinstein S. The position of lysosomes within the cell determines their luminal pH. *J Cell Biol*. 2016;212(6):677-692.
30. Marwaha R, Sharma M. DQ-Red BSA trafficking assay in cultured cells to assess cargo delivery to lysosomes. *Bio Protoc*. 2017;7(19):e2571.
31. von Figura K, Hasilik A. Lysosomal enzymes and their receptors. *Annu Rev Biochem*. 1986;55:167-193.
32. Lu J, Chiang J, Iyer RR, et al. Decreased glucocerebrosidase activity in Gaucher disease parallels quantitative enzyme loss due to abnormal interaction with TCP1 and c-Cbl. *Proc Natl Acad Sci U S A*. 2010;107(50):21665-21670.
33. Wang F, Segatori L. Remodeling the proteostasis network to rescue glucocerebrosidase variants by inhibiting ER-associated degradation and enhancing ER folding. *PLoS One*. 2013;8(4):e61418.
34. Batta G, Soltesz L, Kovacs T, et al. Alterations in the properties of the cell membrane due to glycosphingolipid accumulation in a model of Gaucher disease. *Sci Rep*. 2018;8(1):157.
35. Martina JA, Diab HI, Brady OA, Puertollano R. TFEB and TFE3 are novel components of the integrated stress response. *EMBO J*. 2016;35(5):479-495.
36. Raben N, Puertollano R. TFEB and TFE3: linking lysosomes to cellular adaptation to stress. *Annu Rev Cell Dev Biol*. 2016;32:255-278.
37. Martina JA, Puertollano R. TFEB and TFE3: the art of multi-tasking under stress conditions. *Transcription*. 2017;8(1):48-54.
38. Kim D, Hwang HY, Kim JY, et al. FK506, an immunosuppressive drug, induces autophagy by binding to the V-ATPase catalytic subunit a in neuronal cells. *J Proteome Res*. 2017;16(1):55-64.
39. Roczniak-Ferguson A, Petit CS, Froehlich F, et al. The transcription factor TFEB links mTORC1 signaling to transcriptional control of lysosome homeostasis. *Sci Signal*. 2012;5(228):ra42.
40. Puertollano R. mTOR and lysosome regulation. *F1000Prime Rep*. 2014;6:52.
41. Vega-Rubin-de-Celis S, Pena-Llopis S, Konda M, Brugarolas J. Multistep regulation of TFEB by MTORC1. *Autophagy*. 2017;13(3):464-472.
42. Sancak Y, Bar-Peled L, Zoncu R, Markhard AL, Nada S, Sabatini DM. Ragulator-Rag complex targets mTORC1 to the lysosomal surface and is necessary for its activation by amino acids. *Cell*. 2010;141(2):290-303.
43. Hetz C. The unfolded protein response: controlling cell fate decisions under ER stress and beyond. *Nat Rev Mol Cell Biol*. 2012;13(2):89-102.
44. Mateus D, Marini ES, Progida C, Bakke O. Rab7a modulates ER stress and ER morphology. *Biochim Biophys Acta Mol Cell Res*. 2018;1865(5):781-793.
45. Li M, Baumeister P, Roy B, et al. ATF6 as a transcription activator of the endoplasmic reticulum stress element: thapsigargin stress-induced changes and synergistic interactions with NF-Y and YY1. *Mol Cell Biol*. 2000;20(14):5096-5106.
46. Ma W, Goldberg E, Goldberg J. ER retention is imposed by COPII protein sorting and attenuated by 4-phenylbutyrate. *Elife*. 2017;6:e26624.
47. Lu M, van Tartwijk FW, Lin JQ, et al. The structure and global distribution of the endoplasmic reticulum network are actively regulated by lysosomes. *Sci Adv*. 2020;6(51):eabc7209.
48. Ong DS, Mu TW, Palmer AE, Kelly JW. Endoplasmic reticulum Ca2+ increases enhance mutant glucocerebrosidase proteostasis. *Nat Chem Biol*. 2010;6(6):424-432.
49. Boven LA, van Meurs M, Boot RG, et al. Gaucher cells demonstrate a distinct macrophage phenotype and resemble alternatively activated macrophages. *Am J Clin Pathol*. 2004;122(3):359-369.
50. Barth BM, Shanmugavelandy SS, Tacelosky DM, Kester M, Morad SA, Cabot MC. Gaucher's disease and cancer: a sphingolipid perspective. *Crit Rev Oncog*. 2013;18(3):221-234.
51. Hong YB, Kim EY, Jung SC. Upregulation of proinflammatory cytokines in the fetal brain of the Gaucher mouse. *J Korean Med Sci*. 2006;21(4):733-738.
52. James SP, Stromeyer FW, Chang C, Barranger JA. LIver abnormalities in patients with Gaucher's disease. *Gastroenterology*. 1981;80(1):126-133.
53. Platt FM. Emptying the stores: lysosomal diseases and therapeutic strategies. *Nat Rev Drug Discov*. 2018;17(2):133-150.
54. Barr JE, Munyikwa MR, Frazier EA, Hinton SD. The pseudophosphatase MK-STYX inhibits stress granule assembly independently of Ser149 phosphorylation of G3BP-1. *FEBS J*. 2013;280(1):273-284.
55. Banks DA, Dahal A, McFarland AG, et al. MK-STYX alters the morphology of primary neurons, and outgrowths in MK-STYX overexpressing PC-12 cells develop a neuronal phenotype. *Front Mol Biosci*. 2017;4:76.
56. Dahal A, Hinton SD. Antagonistic roles for STYX pseudophosphatases in neurite outgrowth. *Biochem Soc Trans*. 2017;45(2):381-387.
57. Guardia CM, Farias GG, Jia R, Pu J, Bonifacino JS. BORC functions upstream of kinesins 1 and 3 to coordinate regional movement of lysosomes along different microtubule tracks. *Cell Rep*. 2016;17(8):1950-1961.
58. Cleeter MW, Chau KY, Gluck C, et al. Glucocerebrosidase inhibition causes mitochondrial dysfunction and free radical damage. *Neurochem Int*. 2013;62(1):1-7.
59. de la Mata M, Cotan D, Oropesa-Avila M, et al. Pharmacological chaperones and coenzyme Q10 treatment improves mutant beta-glucocerebrosidase activity and mitochondrial function in neuronopathic forms of Gaucher disease. *Sci Rep*. 2015;5:10903.
60. Gegg ME, Schapira AH. Mitochondrial dysfunction associated with glucocerebrosidase deficiency. *Neurobiol Dis*. 2016;90:43-50.
61. Osellame LD, Rahim AA, Hargreaves IP, et al. Mitochondria and quality control defects in a mouse model of Gaucher disease—links to Parkinson's disease. *Cell Metab*. 2013;17(6):941-953.
62. Singh V, Erady C, Balasubramanian N. Cell-matrix adhesion controls Golgi organization and function through Arf1 activation in anchorage-dependent cells. *J Cell Sci*. 2018;131(16):jcs215855.
63. Mahanty S, Dakappa SS, Shariff R, et al. Keratinocyte differentiation promotes ER stress-dependent lysosome biogenesis. *Cell Death Dis*. 2019;10(4):269.
64. Shakya S, Sharma P, Bhatt AM, Jani RA, Delevoye C, Setty SR. Rab22A recruits BLOC-1 and BLOC-2 to promote the biogenesis of recycling endosomes. *EMBO Rep*. 2018;19(12):e45918.
65. Jani RA, Purushothaman LK, Rani S, Bergam P, Setty SR. STX13 regulates cargo delivery from recycling endosomes during melanosome biogenesis. *J Cell Sci*. 2015;128(17):3263-3276.

66. Filipek PA, de Araujo MEG, Vogel GF, et al. LAMTOR/Ragulator is a negative regulator of Arl8b- and BORC-dependent late endosomal positioning. *J Cell Biol*. 2017;216(12):4199-4215.

SUPPORTING INFORMATION

Additional supporting information can be found online in the Supporting Information section at the end of this article.

How to cite this article: Patel S, Bhatt AM, Bhansali P, Setty SRG. Pseudophosphatase STYXL1 depletion enhances glucocerebrosidase trafficking to lysosomes via ER stress. *Traffic*. 2023;1-16. doi:10.1111/tra.12886